

Timing and resource-aware mapping of quantum circuits to superconducting processors

Lingling Lao,^{1,2,3} Hans van Someren,^{1,2} Imran Ashraf,^{1,2} and Carmen G. Almudever^{1,2}

¹*QuTech, Delft University of Technology, The Netherlands*

²*Department of Quantum and Computer Engineering, Delft University of Technology, The Netherlands*

³*Department of Physics and Astronomy, University College London, UK*

Quantum algorithms need to be compiled to respect the constraints imposed by quantum processors, which is known as the mapping problem. The mapping procedure will result in an increase of the number of gates and of the circuit latency, decreasing the algorithm's success rate. It is crucial to minimize mapping overhead, especially for Noisy Intermediate-Scale Quantum (NISQ) processors that have relatively short qubit coherence times and high gate error rates. Most of prior mapping algorithms have only considered constraints such as the primitive gate set and qubit connectivity, but the actual gate duration and the restrictions imposed by the use of shared classical control electronics have not been taken into account. In this paper, we present a timing and resource-aware mapper called Qmap to make quantum circuits executable on a scalable superconducting processor named Surface-17 with the objective of achieving the shortest circuit latency. In particular, we propose an approach to formulate the classical control restrictions as resource constraints in a conventional list scheduler with polynomial complexity. Furthermore, we implement a routing heuristic to cope with the connectivity limitation. This router finds a set of movement operations that minimally extends circuit latency. To analyze the mapping overhead and evaluate the performance of different mappers, we map 56 quantum benchmarks onto Surface-17. Compared to a prior mapping strategy that minimizes the number of operations, Qmap can reduce the latency overhead up to 47.3% and operation overhead up to 28.6%, respectively.

I. INTRODUCTION

Quantum computing is entering the Noisy Intermediate-Scale Quantum (NISQ) era [1]. This refers to exploiting quantum processors consisting of only 50 to a few hundreds of noisy qubits - i.e. qubits with a relatively short coherence time and faulty operations. Due to the limited number of qubits, hardly or no quantum error correction (QEC) will be used in the next coming years, posing a limitation on the size of the quantum applications that can be successfully run on NISQ processors. Nevertheless, these processors will still be useful to explore quantum physics, and implement small quantum algorithms that will hopefully demonstrate quantum advantage [2]. For running quantum applications on NISQ devices, it is thus crucial to minimize their size in terms of circuit width (number of qubits), number of gates, and circuit latency/depth (number of cycles/steps). In addition, these quantum applications have to be adapted to the hardware constraints imposed by quantum processors. The main constraints include:

- **Primitive gate set:** Generally, only a limited set of quantum gates that can be realized with relatively high fidelity will be predefined on a quantum device. Each quantum technology may support a specific universal set of single-qubit and two-qubit gates, which are called primitive gates. Different primitive gates may have different gate durations. For instance, some superconducting quantum technologies have CZ as a primitive two-qubit gate of which the duration is twice as long as of a single-

qubit primitive gate [3].

- **Qubit connectivity:** quantum technologies such as superconducting qubits [4–6] and quantum dots [7, 8] arrange their qubits in 1D/2D architectures with *nearest-neighbour* (NN) interactions. This means that only neighbouring qubits can interact or in other words, qubits are required to be adjacent for performing a two-qubit gate.
- **Classical control:** classical electronics are required for controlling and operating the qubits. Using a dedicated instrument per qubit is not scalable and is a very expensive approach. Therefore, shared control is required especially when building scalable quantum processors. For instance, a single Arbitrary Waveform Generator (AWG) is used for operating on a group of qubits and several qubits are measured through the same feedline [9, 10].

All these constraints may vary between different quantum processors, and quantum circuits normally cannot be directly executable on these devices. A mapping procedure is required to transform a hardware-agnostic quantum circuit into a constraint-compliant one that can be realized on a given device. This mapping process i) decomposes any quantum gate into the supported primitive gates; ii) performs an initial placement of qubits and finds the set of movement operations to route non-NN qubits to adjacent positions when they need to interact; and iii) schedules operations to leverage the maximum available parallelism. Moreover, minimizing mapping overhead in terms of the number of gates and circuit execution time (latency) is critical for implementing quantum algorithms on NISQ processors.

Different solutions including both exact algorithms and heuristics have been proposed to map quantum circuits onto NISQ processors. [11–15] propose mapping approaches for a 2D grid qubit architecture with NN interactions. Other works [6, 16–26] target current quantum processors from IBM and Rigetti which have irregular qubit connections. Most of prior works [6, 11–23] mainly consider the qubit connectivity and the primitive gate set constraints and their strategies focus on minimizing gate overhead. They assume that any operation takes one time-step without taking the actual gate duration into account. Moreover, they do not consider the shared classical control electronics, which restricts the parallelism of some operations. This means the output circuits from previous mapping algorithms need to be further scheduled by another hardware-aware translation phase such as OpenPulse from IBM [10] so that quantum operations can be performed on real qubits with correct timing without violating any classical control constraint [10, 27]. Venturelli et al. [24–26] consider gate duration and crosstalk constraints, but their mathematical optimization formulation has exponential complexity.

This paper presents a timing and resource-aware mapper called **Qmap** to make quantum circuits executable on the Surface-17 superconducting processor [27]. Different modules are developed in Qmap to comply with the hardware constraints, including common restrictions such as primitive gate set and qubit connectivity, as well as other hardware parameters such as actual gate duration and classical control constraints which have not been addressed in prior works. Qmap is embedded in the OpenQL compiler [28] and its output circuit is described by an executable low-level QASM-like code with precise timing information. In order to analyze the impact of the mapping procedure, we compile 56 benchmarks taken from RevLib [29] and QLib [30] onto the Surface-17 processor. Compared to the original circuit characteristics before mapping, the evaluation results show that the circuit latency and the number of operations after mapping can increase up to 260% and 78.1%, respectively.

The main contributions of this paper are the following:

- We provide a comprehensive analysis of the hardware constraints of the Surface-17 processor, including the supported primitive gates with corresponding duration, the processor’s topology that limits the qubit connectivity, and the classical control constraints resulting from the shared control electronics among qubits.
- We develop a Qmap mapper embedded in the OpenQL compiler [28] to compile a quantum circuit into one that complies with all the above constraints of Surface-17. Specifically, we propose an approach to formulate the classical control limitations as resource constraints in a conventional list scheduling algorithm. Its objective is to achieve the shortest circuit latency and therefore the highest gate-level parallelism with respect to these con-

straints. The complexity of the developed scheduling heuristic is polynomial in terms of the number of operations and resources, which is applicable to large-scale circuits.

- For coping with the limited qubit connectivity, we present a routing strategy in Qmap to move qubits that need to interact to be adjacent. The proposed router not only finds shortest paths that use least number of operations for moving qubits (which is the routing strategy developed in prior works) but also selects a set of movement operations that will minimally extend the overall circuit latency. Compared to a prior mapping strategy, the average reduction of latency overhead and the average reduction of gate overhead when using Qmap are 22% and 3.0%, respectively.
- To enable a flexible implementation, we provide a method to encode all hardware characteristics in a configuration file that is accessed by every module of the compiler. This flexibility also allows a comparative analysis of the mapping impacts of different characteristics, giving some directions for building future quantum devices. In addition, it allows the mapper to target different processors.
- Qmap uses not only SWAP operations (3 consecutive CNOTs) for moving qubits but also MOVE operations (2 consecutive CNOTs) when possible. Compared to the mapping by only using SWAPs in prior works, the use of MOVEs helps to reduce the number of gates and the circuit latency up to 38.9% and 29% respectively.

The rest of this paper is organized as follows. We first describe all the hardware parameters that will be considered in this work in Section II. Then we introduce the proposed resource-constrained scheduling algorithm in Section III and other modules of the developed mapper such as the routing heuristic in Section IV. Afterwards, we evaluate this mapping strategy in Section V and summarize related works in Section VI. Finally, Section VII concludes the paper and discusses future work.

II. QUANTUM HARDWARE CONSTRAINTS

In this section, the hardware constraints of the Surface-17 superconducting processor will be briefly introduced, including the primitive gates that can be directly performed, the topology of the processor which limits interactions between qubits, and the constraints caused by the classical control electronics which impose extra limitations on the parallelism of the operations.

A. Primitive gate set

In order to run any quantum circuit, a universal set of operations needs to be implemented. In superconducting quantum processors, these operations commonly are measurement, single-qubit rotations, and multi-qubit gates.

In principle, any kind of single-qubit rotation can be performed on the Surface-17 processor. However, an infinite amount of gates cannot be predefined. In this work, we will limit single qubit gates to X and Y rotations (easier to implement), and more specifically ± 45 , ± 90 and ± 180 degrees will be used in our decomposition. The primitive two-qubit gate on this processor is the conditional-phase (CZ) gate. Table I shows the gate duration (gate execution time) of single-qubit gates, CZ gate and measurement (in the Z basis) [31]. After mapping, the output circuit will only contain operations that belong to this primitive gate set. The decomposition for Z, H, S, S^\dagger , T, T^\dagger , CNOT, SWAP and MOVE gates into these primitive gates is shown in Figure 1 (ignoring the global phase).

TABLE I: The gate duration in cycles (each cycle represent 20 nanoseconds) of the primitive gates in the Surface-17 processor.

Gate type	Duration
$R_X(\pm 45, \pm 90, \pm 180)$	1 cycle
$R_Y(\pm 45, \pm 90, \pm 180)$	1 cycle
CZ	2 cycles
M_Z	15 cycles

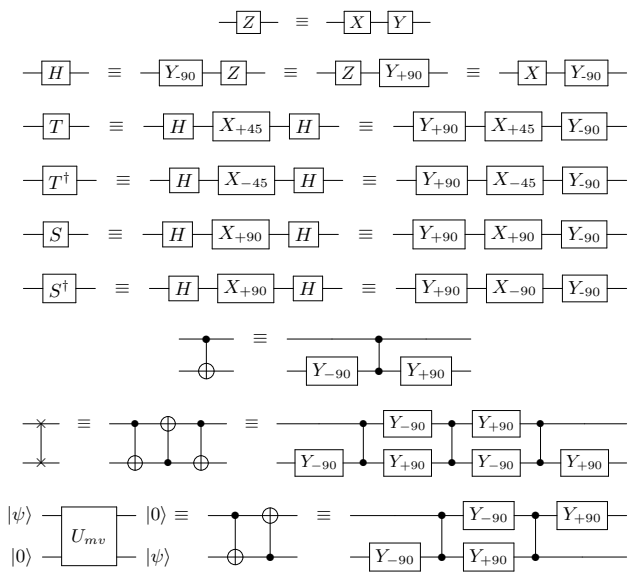


FIG. 1: Gate decomposition into primitives supported in the superconducting Surface-17 processor. U_{mv} is the MOVE operation.

B. Processor topology

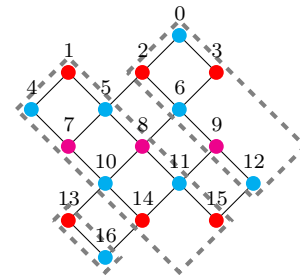


FIG. 2: Schematic of the realization of Surface-17 superconducting processor.

Figure 2 shows the topology of the Surface-17 processor, where nodes represent the qubits and edges represent the connections (resonators) between them. Two-qubit gates can only be performed between connected qubits, i.e., *nearest-neighbouring* qubits. This implies that qubits that have to interact but are not placed in neighbouring positions will need to be moved to be adjacent. Quantum states in superconducting technology are usually moved using SWAP gates. A SWAP gate is implemented by three CNOTs that in the case of the Surface-17 processor need to be further decomposed into CZ and R_Y gates as shown in Figure 1. In this work, we also consider the use of a MOVE operation which only requires two CNOTs (see Figure 1). Note that a MOVE operation requires that the destination qubit where the quantum state needs to be moved to, is in the $|0\rangle$ state. As mentioned, moving qubits results in an overhead in terms of number of operations and circuit depth, which in turn will decrease the circuit reliability. Therefore, an efficient routing procedure is required to find the series of movement operations to enable all two-qubit gates with minimum overhead.

C. Classical control constraints

In principle, any qubit in a processor can be operated individually and then any combination of independent single-qubit and two-qubit operations can be performed in parallel. However, scalable quantum processors use classical control electronics with channels that are shared among several qubits. Here we will describe the constraints imposed by the classical control electronics used in the Surface-17 processor and how they affect the parallelism of quantum operations.

a. Single-qubit gates: Single-qubit gates on superconducting qubits are performed by using microwave pulses. In Surface-17, these pulses are applied at a few fixed specific frequencies to ensure scalability and precise control. The three frequencies used in Surface-17 are shown in Figure 2: single-qubit gates on red, blue and pink colored qubits are performed at frequencies f_1 ,

f_2 , and f_3 , respectively [27]. In this work, we assume that same-frequency qubits are operated by the same microwave source or arbitrary waveform generator (AWG) and a vector switch matrix (VSM) is used for distributing the control pulses modulated on the waves to the corresponding qubits [9].

The consequence of this is that one can perform the same single-qubit gate on all or some of the qubits that share a frequency, but one cannot perform different single-qubit gates at the same time on these qubits (as these would require other pulses to be generated). For instance, an X gate can be performed simultaneously on any of the pink qubits (7, 8 and 9) but not an X and a Y operation.

b. Measurement: Measuring the qubits is done by using feedlines each of which is coupled to multiple qubits [27]. In Figure 2, qubits in the same dashed rectangle are using the same feedline, e.g., qubits 13 and 16 will be measured through the same feedline. Because measurement takes several steps in sequence, measurement of a qubit cannot start when another qubit coupled to the same feedline is being measured, but any combination of qubits that are coupled to the same feedline can be measured simultaneously at a given time. For instance, qubits 13 and 16 can be measured at time t_0 , but it is not possible to start measuring qubit 13 at time t_0 and then measure qubit 16 at time t_1 if the previous measurement has not finished.

c. Two-qubit gates: As mentioned, in the processor of Figure 2 each qubit belongs to one of three frequency groups $f_1 > f_2 > f_3$, colored red, blue and pink, respectively; links between neighbouring qubits are either between qubits from f_1 and f_2 , or between qubits from f_2 and f_3 , i.e. between a higher frequency qubit and a next lower one. In between additional frequencies are defined: $f_1 > f_1^{int} > f_2 > f_2^{park} > f_2^{int} > f_3 > f_3^{park}$ (see the frequency arrangement and the example interactions presented in Figure 5 of [27]); each qubit can be individually driven with one of the frequencies of its group (e.g. group $\{f_2, f_2^{int}, f_2^{park}\}$). A CZ gate between two neighbouring qubits is realized by lowering the frequency of the higher frequency qubit near to the frequency of the lower one. For instance, a CZ gate between qubits 3 and 0 is performed by detuning qubit 3 from f_1 to f_1^{int} , which is near to the frequency f_2 of qubit 0. However, CZ gates will occur between any two neighbouring qubits which have close frequencies and share a connection. For example, a CZ gate can occur between the detuned qubit 3 in f_1^{int} and its neighbour qubit 6 in f_2 in the above example. To avoid this, the qubits that should not be involved in a CZ gate must be kept out of the way. In this example, q6 needs to be detuned to a lower *parking frequency*, f_2^{park} . Note that, qubits in parking frequencies cannot engage in any two-qubit or single-qubit gate. In addition, when performing a CZ on qubits 3 and 0, qubit 2 must stay at f_1 (and not be detuned) to avoid interaction between qubits 2 and 0. The implementation of two-qubit gates poses limitations not only on parallelizing multiple two-

qubit gates but also on the parallelism of two-qubit gates and single-qubit gates. More details can be found in [27].

Violation of these classical control constraints will cause incorrect execution of quantum operations, leading to a computational failure. Therefore, scheduling algorithms that can take these constraints into account are needed to explore the maximum available parallelism.

D. Configuration file

The hardware characteristics explained in this section are precisely described in a configuration file (in json format). It parameterizes the mapping modules that will be introduced in the next section.

a. Primitive gate set: For Surface-17, the primitive gates with all attributes including duration as listed in Table I and the gate decomposition rules corresponding to those in Figure 1 are described in full detail in the configuration file.

b. Processor topology: The topology is defined by describing each connection with its source and target qubits. In Surface-17, all edges are bidirectional, e.g., both $\text{CNOT}(q_a, q_b)$ and $\text{CNOT}(q_b, q_a)$ can be performed on edge $e(q_a, q_b)$. Qubits and directed qubit connections are both named by integer values taken from contiguous ranges of integer numbers starting from 0. As an example, the qubit numbering of the Surface-17 processor is shown in Figure 2; in the Surface-17 topology the number of directed qubit connections is 48.

c. Classical control constraints: For **single-qubit gates**, we use a look-up table T_{g1} to describe the available AWGs and the list of corresponding qubits that each AWG controls. Similarly for **measurement**, the feedlines (three feedlines in Surface-17) and the corresponding qubits that each feedline is coupled to are described in a look-up table T_{gm} in the configuration file. The AWGs and feedlines are both named by contiguous integer numbers starting from 0. As mentioned in Section II, it is assumed that three AWGs and three feedlines are used in Surface-17, that is, $|T_{g1}| = 3$ and $|T_{gm}| = 3$, respectively. The classical control constraints of **two-qubit gates** are defined by using two look-up tables. One called T_{g2f} describes for each connection which other connections cannot be used to execute CZ gates in parallel (24 bi-directional edges on the Surface-17 topology, i.e. $|T_{g2f}| = 48$). The other table T_{g2d} describes for each connection which set of qubits needs to be detuned in addition to one of its end-points, which means a CZ on this connection and single-qubit gates on these detuned qubits cannot be performed in parallel ($|T_{g2d}| = 48$).

III. RESOURCE-CONSTRAINED SCHEDULING

Some current quantum technologies such as superconducting qubits and quantum dots have relatively short coherence times, limiting the size of circuits that can be

run successfully with high fidelity. It is therefore necessary to minimize the execution time of the circuit (or *makespan*, or circuit latency) and explore the highest gate-level parallelism, which is the objective of a quantum gate scheduler. Before discussing the other mapping modules, we first introduce the proposed heuristic scheduling algorithm that can take the actual gate duration and classical control constraints into account. The circuit shown in Figure 3 will be used as an example. We refer to the qubits in the quantum circuit as virtual qubits (others call them program qubits or logical qubits). These need to be mapped to the qubits in the quantum processor called physical, real or hardware qubits or locations

A. Weighted dependency graph

As mentioned previously, precise timing is essential for correctly executing quantum applications on real qubits. Therefore, a scheduler that considers gate duration is required to efficiently generate the correct instruction sequences with timing information meanwhile minimizing the circuit execution time. Prior works [6, 11–23] do not consider the actual gate duration, assuming any operation takes one time-step. To ensure quantum operations can be executed at correct time, their output circuits need to be further scheduled by some other low-level hardware-aware units such as OpenPulse [10]. In contrast, the scheduling algorithm developed in the Qmap mapper will directly take gate duration into account.

Similar to classical scheduling, a Quantum Operation Dependency Graph (QODG) $G(V_G, E_G)$ is constructed from the QASM representation of a quantum circuit, in which each operation is denoted by a node $v_i \in V_G$, and the data dependency between two operations v_i and v_j is represented by a directed edge $e(v_i, v_j) \in E_G$ with weight w_i that represents the duration of operation v_i . Pseudo source and sink nodes are added to the start and end to simplify starting and stopping iteration over the graph. The QODG of the circuit in Figure 3a is shown in Figure 4a. In previous works that do not consider gate duration, only directed graphs are constructed, which cannot be directly applied to this work.

B. Formulation of resource constraints

Furthermore, the scheduler also needs to adhere to the parallelism restrictions imposed by the shared classical control electronics as described in Section II. In this work, these classical control constraints are treated as resource constraints in an otherwise conventional critical path list-scheduler implementation [32]. A so-called machine state S is defined to describe the occupation status of each resource $r_i \in R$, where R represents the set of all resources in T_{g1}, T_{gm}, T_{g2f} , and T_{g2d} . The constraints for *single-qubit gates* and *measurement* are implemented by using

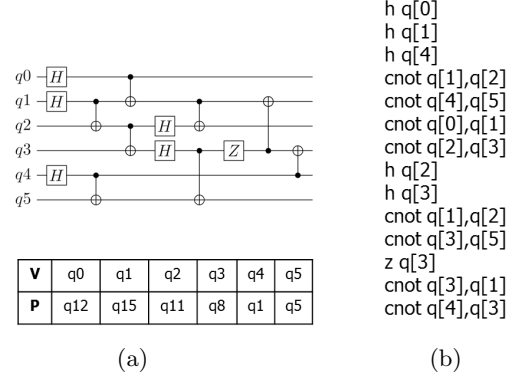


FIG. 3: An example circuit consisting of 6 qubits and 15 gates. (a) Its circuit description (top) and its virtual to physical qubits mapping (bottom) for the Surface-17 processor after initial placement; (b) Its cQASM representation without scheduling.

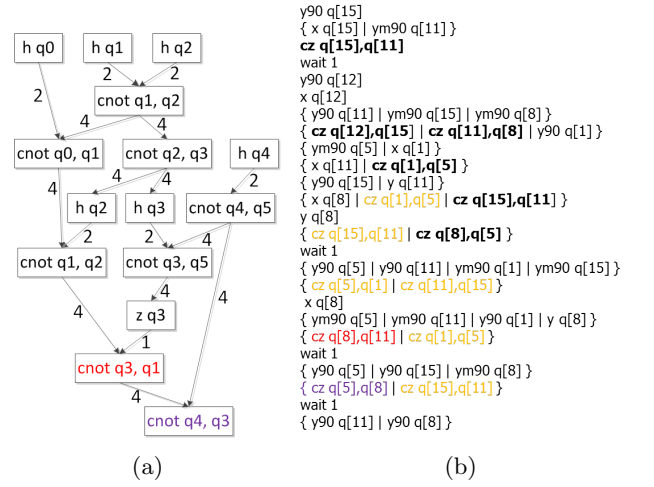


FIG. 4: (a) The QODG of the circuit in Figure 3a. The red and purple boxed CNOTs have qubits that are not NN. (b) The parallel cQASM code of the mapped circuit, where each line represents one cycle and operations in the same line (inside one bracket) are scheduled to start at the same cycle. The CZ gates in bold are already nearest neighbouring. Movement operations (added two-qubit gates are in yellow) are inserted to perform the CZ gates in red and purple.

$|T_{g1}|$ and $|T_{gm}|$ resource states, respectively. To support the *two-qubit gates* constraint, there is a resource state for each connection (to constrain mutual CZ concurrency) and a resource state per qubit (to constrain CZ versus single-qubit gate concurrency). Specifically, a resource state consists of two elements: the operation type that is using this resource and the occupation period which is described by a pair of cycle time (t_0, t_1) , representing the first cycle that it is occupied and the first cycle that it is free again, respectively. If an operation v is sched-

uled at cycle t_0 ($v.cycle = t_0$), then all the resources for performing v ($v.resources$) will be occupied till (and not including) $t_1 = t_0 + v.duration$ ($v.duration$ is the duration of v).

Algorithm 1 Forward Scheduling algorithm

Input: Non-scheduled circuit

Input: Configuration file with gate durations and resource descriptions R

Output: Scheduled circuit

```

1: Generate QODG  $G(V_G, E_G)$  from circuit
2: Initialize  $\forall v \in V_G : v.resources \subset R$  and  $v.duration$ 
3:  $V_m \leftarrow$  Unique pseudo source node
4:  $V_{av} \leftarrow$  All available gates in  $G(V_G - V_m, E_G)$ 
5: Initialize cycle  $t \leftarrow 0$ 
6: Initialize machine-state  $S \leftarrow \forall r \in R$  is free
7: while  $V_{av} \neq \emptyset$  do
8:    $V_r \leftarrow$  resource-free gates  $\subset V_{av}$  based on  $S$ 
9:   if  $V_r \neq \emptyset$  then
10:     $V_c \leftarrow$  Most-critical gates  $\subset V_r$  in  $G(V_G - V_m, E_G)$ 
11:    Select  $v \in V_c$  which is first in the circuit
12:    Add  $v$  to  $V_m$ 
13:     $v.cycle \leftarrow t$ 
14:    Update  $S$  with  $v.resources$  occupied at  $[t, t + v.duration)$ 
15:     $V_{av} \leftarrow$  All available gates in  $G(V_G - V_m, E_G)$ 
16:   else
17:     $t \leftarrow t + 1$ 
18:   end if
19: end while

```

C. Scheduling heuristic

Algorithm 1 shows the pseudo code of this algorithm, which schedules all the gates of a given circuit with respect to the resource constraints. Its objective is to achieve the shortest circuit latency.

The heuristic maintains two sets of gates: V_m holds the gates that have been scheduled, and V_{av} includes the gates that are available for scheduling. A gate v is **available** when all predecessors p of v in G have been scheduled, that is, $\forall p, p$ is in V_m . Furthermore, it maintains a machine-state S consisting of all resource states as described above.

Algorithm 1 first generates a QODG for the input circuit and initializes V_m , V_{av} , and S (lines 1-6). After finding all the available gates at current cycle t , it selects the ones that can be scheduled at cycle t and collects them in V_r (line 8). A gate $v \in V_{av}$ can be scheduled at cycle t only if it is **resource-free** at t : when its predecessors have finished execution, i.e., $\forall p \in V_m, p.cycle + p.duration \leq t$ (this data dependency constraint can be seen as qubit resource constraint); and when all resources in $v.resources$ are not occupied for all cycles in $[t, t + v.duration)$. The worst-case time complexity of this step is $O(\min(g, n) \cdot (n + |R|))$, n and g are the number of qubits and operations in the input circuit, respectively (in the worst case, gates on every qubit can be scheduled.).

If V_r is not empty, the heuristic selects the first most-critical gate v in this set (lines 9-11). A most-critical gate in V_r is the one that has the longest path to the pseudo sink node of the QODG G . In this work, the length of the longest path is pre-computed for each node in G , which only takes linear time. Then it adds this gate v to V_m , assigns the current cycle attribute to $v.cycle$, updates S by reserving all the resources of v ($v.resources$) for its execution duration, and updates V_{av} given that v has been scheduled now and thus some more gates may have become available (lines 12-15). In this case, cycle t is not incremented because more gates may be scheduled in the same cycle.

If V_r is empty, the heuristic increments t (line 17) and continues the schedule loop again until all the gates are scheduled, that is, V_{av} is empty. In the worst case, this loop needs to be repeated $O(L)$ times, L is the multiplication of the total number of operations (g) in the given circuit and the longest gate duration in cycles. Resource-constrained scheduling is NP-hard in the strong sense [33]. Previous works that are using exact optimization approaches or exhaustive search algorithms for scheduling [12, 17, 18, 24] cannot be adapted to efficiently solve this problem. In contrast, the proposed scheduling algorithm has reduced its complexity to at most

$$O_{schedule} = O(\min(g, n) \cdot (n + |R|) \cdot g).$$

IV. MAPPING QUANTUM ALGORITHMS

Mapping means to transform the original hardware-agnostic quantum circuit that describes the quantum algorithm to an equivalent one that can be executed on the target quantum processor. To this purpose, the mapping process has to be aware of the constraints imposed by the physical implementation of the quantum processor. These include the set of primitive gates that is supported, the allowed qubit interactions that are determined by the processor topology, and the limited concurrency of multi-gate execution because of classical control constraints. Mapping will likely increase the number of operations that are required to implement the given algorithm as well as the circuit latency/depth, decreasing the reliability of the algorithm. Efficient algorithms that can minimize this mapping overhead are then necessary, especially in NISQ processors where noise sets a limit on the maximum size of a computation that can be run successfully.

A. Overview of the Qmap mapper

The **Qmap** mapper developed in this work is embedded in the OpenQL compiler [28] and its design flow is shown in Figure 5. The input of Qmap is a quantum circuit written in OpenQL (C++ or Python). The OpenQL compiler reads and parses it to a QASM-level intermediate representation. Qmap then performs the mapping

and optimization of the quantum circuit based on the processor characteristics provided in a configuration file as described in the previous section. This approach allows Qmap to target different quantum devices by just changing the parameters in the configuration file. After mapping, QASM-like code is generated. Currently, the OpenQL compiler is capable of generating cQASM [34] that can be executed on the QX simulator [35] as well as eQASM [36], a QASM-like executable code that can target the Surface-17 processor. The generation of other QASM-like languages will be part of future extensions of the OpenQL compiler. The modules of Qmap will be discussed in the rest of this section.

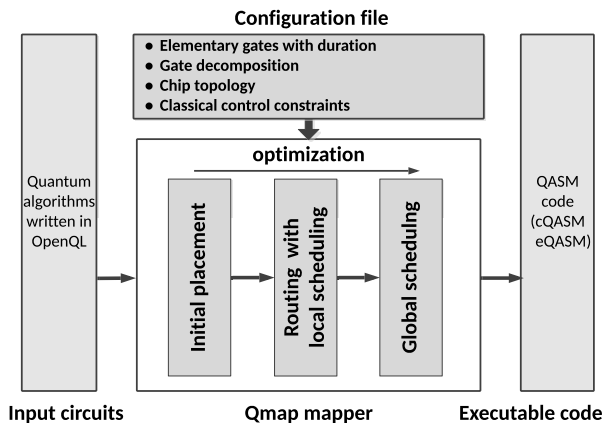


FIG. 5: Overview of the Qmap mapper embedded in the OpenQL compiler.

B. Initial placement

It is preferable to place highly interacting qubits next to each other such that less movement operations will be added for performing two-qubit gates. Similar to the placement approaches in [37], the initial placement problem in this work is formulated as a quadratic assignment problem (QAP) and the objective is to minimize the movement or communication overhead, which is modeled by the distance between interacting qubits minus 1. Qmap tries to find an initial placement with minimum communication overhead by using the Integer Linear Programming (ILP) algorithm presented in [38]. Such an initial placement implementation can only solve small-scale problems in reasonable time. Even though for near-term implementations these numbers largely suffice, for large-scale circuits, one can either partition a large circuit into several smaller ones or apply heuristic algorithms to efficiently solve these models [39]. Other works also solve this initial placement problem by using a Satisfiability Modulo Theories (SMT) solver [40].

C. Qubit Router

It is unlikely to find an initial placement in which all the qubit pairs that a two-qubit gate need to be performed on can be placed in neighboring positions. Therefore, qubits will have to be moved during computation. For instance, based on the initial placement of qubits shown in Figure 3a, the first 6 CNOT gates of the circuit can be performed directly as qubits are NN, but qubits in the last 2 CNOT gates will need to be routed to adjacent positions. Routing refers to the task of finding a series of movement operations that enables the execution of two-qubit gates on a given processor topology with low communication overhead. To do so, multiple routing paths are evaluated and one is selected based on various optimization criteria such as the number of added movement operations, increase of circuit depth, or decrease of circuit reliability [6, 16–22, 24, 40, 41]. Afterwards, the corresponding movement operations are inserted.

Algorithm 2 Forward Routing algorithm

Input: Non-routed circuit, VP-map M

Input: Configuration file with topology and constraints

Output: Routed circuit

- 1: Generate QODG $G(V_G, E_G)$
 - 2: $V_m \leftarrow$ Unique pseudo source node
 - 3: $V_{av} \leftarrow$ All available gates in $G(V_G - V_m, E_G)$
 - 4: **while** $V_{av} \neq \emptyset$ **do**
 - 5: $V_{nn} \leftarrow$ All single-qubit and NN two-qubit gates in V_{av}
 - 6: **if** $V_{nn} \neq \emptyset$ **then**
 - 7: Select the first most-critical gate $v \in V_{nn}$
 - 8: **else**
 - 9: $V_c \leftarrow$ Most-critical gates $\subset V_{av}$ in $G(V_G - V_m, E_G)$
 - 10: Select $v \in V_c$ which is first in the circuit
 - 11: Insert movement(s) for v
 - 12: Update M
 - 13: **end if**
 - 14: Map v according to M
 - 15: Add v to V_m
 - 16: $V_{av} \leftarrow$ All available gates in $G(V_G - V_m, E_G)$
 - 17: **end while**
-

1. Routing heuristic

In this work, after the ILP-based initial placement, a heuristic algorithm is used to perform this routing task. It is a scheduler-based heuristic of which the objective is to minimize overall circuit latency. Algorithm 2 shows the pseudo code of the proposed routing algorithm, which finds all two-qubit gates in which qubits are not nearest-neighbours and inserts the required movement operations to make them adjacent. As mentioned in Section II we use SWAPs as well as MOVE operations for moving qubits.

The router algorithm starts by mapping the pseudo source node and then selecting all available gates (V_{av}) from the generated QODG (lines 1-3). Then it finds all the single-qubit gates and the two-qubit gates of which

qubits are NN from V_{av} , these gates are collected in V_{nn} (line 5). If V_{nn} is not empty, then all gates in this set are mapped directly and a new set of available gates is computed (lines 6, 7, and 13-15). Mapping a (NN) gate implies replacing virtual qubit operands by their physical counterparts according to the VP-map table M similar to the one shown in Figure 3a and decomposing this gate to its primitives when the configuration specifies so.

After that, only non-NN two-qubit gates remain in the available set. The router selects the ones which are most critical in the remaining dependency graph G since they have the highest likelihood to extend the circuit when mapped in an inefficient way or when delayed (line 9). When there are several equally critical gates, the routing heuristic chooses the first one in the input circuit (line 10) and finds a set of movement operations to bring these two qubits to adjacent positions. After the movement set selection, the router schedules the SWAP/MOVE operations into the circuit (line 11), updates the VP-map (line 12), recomputes the set of available gates (line 15), and runs the routing heuristic until all the gates are mapped.

2. Movement set selection

For finding a set of movement operations for a non-NN two-qubit gate, all shortest paths between these two qubits are considered. During Qmap initialization time, the distance (i.e. the length of the shortest path) between each pair of qubits has been computed using the Floyd-Warshall algorithm. Finding all shortest paths between qubits at mapping-time is done by a breadth-first search (BFS), that is, selecting only path extensions which decrease the distance between the qubits. For each shortest path, there may exist several movement sets since qubits can meet in any neighboring position within the path. Note that all movement sets would lead to adding an equal minimum number of movements to the circuit. In a $\sqrt{N} \times \sqrt{N}$ grid architecture, the total number of shortest paths between most remote two nodes (q_i, q_j) is $O(4^{\sqrt{N}})$ and the number of movement sets for each path is $(2\sqrt{N} - 2)$.

In this work, a set of movement operations that minimally extends the circuit latency is selected and scheduled into the circuit. As shown in Algorithm 3, this router evaluates all movement sets by looking back to the previously mapped gates (lines 1 and 2) and interleaving each set of movements with those gates using the proposed resource-constrained scheduling heuristic (Section III) in an as-soon-as-possible (ASAP) policy (line 4). It selects the one(s) which minimally extend(s) the circuit latency (lines 6 and 7). When there are multiple minimal-cost sets, a random one is taken. The complexity of this routing strategy is $O(g\sqrt{n}4^{\sqrt{n}}) \cdot O_{schedule}$.

Algorithm 3 Movement selection algorithm

Input: QODG $G(V_G, E_G)$, gate v , VP-map M

Input: Configuration file with topology and constraints

Output: The set of movements for v

```

1:  $P \leftarrow$  All shortest paths for  $v$ 
2:  $MV_P \leftarrow$  All possible sets of movements based on  $P$ 
3: for  $mv_j$  in  $MV_P$  do
4:   Interleave  $mv_j$  with previous gates (looking back)
5:    $L_{mv_j} \leftarrow$  circuit's latency extension by  $mv_j$ 
6: end for
7: if  $L_{mv_i} = \min(\bigcup_j L_{mv_j})$  then
8:   Select  $mv_i$  as the set of movements, picking a random
   minimum one when there are more
9: end if

```

D. Global scheduling

After routing, the circuit adheres to the processor topology constraint for two-qubit interactions and has been scheduled in an as-soon-as-possible (ASAP) way. The global scheduler reschedules the routed circuit to achieve the shortest circuit latency and the highest instruction-level parallelism. It does this in an as-late-as-possible (ALAP) way to minimize the required life-time and thus the decoherence error of each qubit. The global scheduler employs a backward version of Algorithm 1, i.e. it traverses the circuit starting from the sink node, working backwards through the circuit and decrementing t .

E. Decomposition and optimization

Starting from a quantum circuit described in cQASM format (see Figure 3), the circuit is also decomposed during mapping into one which only contains the *primitive gates* specified in the configuration file, on top of adherence to the other constraints. A circuit optimization module is also implemented to reduce the number of gates, e.g., two consecutive X gates can cancel each other out.

The decomposition and optimization can be done at every step of the mapping procedure, i.e. before, during, and after routing. Qmap reduces sequences of single qubit gates to their minimally required sequence both before and after routing. Whether decomposition is applied at a mapping step is specified in the configuration file. The implementation of the QODG represents the commutability of not only all gates with disjoint qubit operands but also the known two-qubit operations CNOT and CZ with overlapping operands, and optimizes their order during both routing and global scheduling.

The mapped version of the circuit in Figure 3a by using the Qmap mapper is shown in Figure 4b. It is described in cQASM code with precise timing information, that is, which operations can be issued at each cycle. The output circuit can also be represented by eQASM code [36] that

can be directly read by the quantum microarchitecture in [42].

V. QMAP EVALUATION

In this section, we evaluate *Qmap* by mapping a set of benchmarks from RevLib [29] and QLib [30] on the superconducting processor Surface-17 that has a distance-3 surface-code topology [27]. All the hardware constraints discussed in Section II, including the primitive gates with their real gate duration, the topology and the electronic control constraints are taken into account. The mapping experiments are executed on a server with 2 Intel Xeon E5-2683 CPUs (56 logical cores) and 377GB memory. The Operating System is CentOS 7.5 with Linux kernel version 3.10 and GCC version 4.8.5.

A. Benchmarks

The circuit characteristics of the used benchmarks are shown in Table II. All circuits have been decomposed into ones which only consist of gates from the universal set {Pauli, S , S^\dagger , T , T^\dagger , H , CNOT}. In these benchmarks, the number of qubits varies from 3 to 16, the number of gates goes from 5 to 64283, and the percentage of CNOT gates varies from 2.8% to 100%. Moreover, the minimum circuit depth and the minimum circuit latency are also included, ranging from 2 to 35572 time-steps and from 5 to 12256 cycles (using the gate duration of Surface-17), respectively. Note that these numbers are meant to characterize the algorithms without considering the processor topology and classical control constraints.

The latter two parameters are defined as follows:

Circuit depth is the length of the circuit. It is equivalent to the total number of time-steps for executing the circuit assuming each of the gates takes one time-step.

Circuit latency refers to the execution time of the circuit considering the real gate duration. Latency and gate duration are expressed in cycles. In this paper, we assume that a cycle takes 20 nanoseconds.

In order to generate quantum circuits which are executable on real processors, extra movement operations need to be added and gate parallelism will be compromised. Other parameters after mapping these benchmarks to the Surface-17 processor are obtained, such as the number of inserted SWAP and MOVE operations and the CPU time the mapping process takes. We analyze the impact of the mapping procedure in terms of number of gates and circuit latency for Surface-17. The mapping overhead is calculated by $(X_o - X_{in})/X_{in}$, where X_{in} and X_o represent the values of the same circuit characteristic before and after mapping, respectively.

B. Prior mapping strategies

As mentioned previously, the routing algorithms in most of prior works [6, 11–23] optimise the number of operations, that is, the number of added SWAP gates. They do not take actual gate duration and classical control limitations into account. Their output circuits need to be further scheduled by a low-level hardware unit like OpenPulse [10] such that they can be correctly executed with precise timing. In this work, we also implement such a mapping procedure called **MinPath** mapper to compare with the proposed timing and resource-aware *Qmap* that considers gate duration and control constraints during routing to minimize the circuit latency. **MinPath** uses the same initial placement approach as the *Qmap* mapper. However, the router in **MinPath** randomly selects one of the movement sets along one of the shortest paths as described in Section IV C without respecting to classical control constraints and without evaluating which set(s) will minimally extend circuit latency. The complexity of the router in **MinPath** is $O(g\sqrt{n}4^{\sqrt{n}})$.

Furthermore, we also introduce a **Trivial** mapper that may not be able to map the circuit with minimal latency extension but its routing strategy has linear complexity ($O(g)$). In the trivial mapping strategy, a naive initial placement is used in which qubits are just placed in their appearing order, no circuit optimization is performed. For the router in the trivial mapper, the gates in the input circuit are mapped in the order as they appear in the circuit, i.e. by-passing the QODG. For performing a non-NN two-qubit gate, it simply selects the first shortest path that is found. Moreover, only a single set of movement operations is generated for the chosen path, the set moving the control qubit adjacent to the target qubit. In addition, only SWAP gates are generated for moving qubits. After routing, the proposed resource-constrained scheduling will be applied. By contrast, the **MinPath** and *Qmap* mappers use the ILP-based initial placement, enable circuit optimization, and can insert both SWAP and MOVE gates.

The main differences of these three mapping strategies are summarized in Table III. To provide gate sequences with precise timing and comply with the classical control constraints, the proposed resource-constrained scheduling is also performed after routing procedure of the **Trivial** and **MinPath** mappers.

C. Overhead comparison of different mappers

Table IV shows the results of mapping benchmark circuits to the Surface-17 superconducting processor using three different mapping strategies: **Trivial**, **MinPath**, and *Qmap*. In this paper, the mapper is set to only find an ILP-based initial placement for the first ten two-qubit gates in any given circuit and computation time is limited to 10 minutes and is not included in the final CPU time. For each benchmark circuit, the mapping proce-

TABLE II: The characteristics of the input benchmarks including the number of qubits, the total number of gates, the number of two-qubit gates (CNOTs), its circuit depth and its circuit latency in cycles (20 ns per cycle).

Benchmarks	Qubits	Gates	CNOTs	Depth	Latency	Benchmarks	Qubits	Gates	CNOTs	Depth	Latency
alu_bdd_288	7	84	38	48	169	sym9_146	12	328	148	127	450
alu_v0_27	5	36	17	21	72	sys6_v0_111	10	215	98	74	266
benstein_vazirani	16	35	1	5	40	vbeAdder_2b	7	210	42	52	116
4gt12_v1_89	6	228	100	130	448	wim_266	11	986	427	514	1788
4gt4_v0_72	6	258	113	137	478	xor5_254	6	7	5	2	5
4mod5_bdd_287	7	70	31	40	140	z4_268	11	3073	1343	1643	5688
cm42a_207	14	1776	771	940	3249	adr4_197	13	3439	1498	1839	6377
cnt3.5_180	16	485	215	207	729	9symml_195	11	34881	15232	19235	66303
cuccaroAdder_1b	4	73	17	25	58	clip_206	14	33827	14772	17879	61786
cuccaroMultiply	6	176	32	55	133	cm152a_212	12	1221	532	684	2366
decod24_bdd_294	6	73	32	40	143	cm85a_209	14	11414	4986	6374	21967
decod24_enable	6	338	149	190	669	co14_215	15	17936	7840	8570	29608
graycode6_47	6	5	5	5	20	cycle10_2_110	12	6050	2648	3384	11692
ham3_102	3	20	11	11	41	dc1_220	11	1914	833	1038	3597
millar_11	3	50	23	29	105	dc2_222	15	9462	4131	5242	18097
mini_alu_167	5	288	126	162	564	dist_223	13	38046	16624	19693	68111
mod5adder_127	6	555	239	302	1048	ham15_107	15	8763	3858	4793	16607
mod8_10_177	6	440	196	248	872	life_238	11	22445	9800	12511	43123
one_two_three	5	70	32	40	141	max46_240	10	27126	11844	14257	49400
rd32_v0_66	4	34	16	18	66	mini_alu_305	10	173	77	68	242
rd53_311	13	275	124	124	441	misex1_241	15	4813	2100	2676	9240
rd73_140	10	230	104	92	330	pm1_249	14	1776	771	940	3249
rd84_142	15	343	154	110	394	radd_250	13	3213	1405	1778	6163
sf_274	6	781	336	436	1516	root_255	13	17159	7493	8835	30575
shor_15	11	4792	1788	2268	7731	sqn_258	10	10223	4459	5458	18955
sqrt8_260	12	3009	1314	1659	5740	square_root_7	15	7630	3089	3830	13049
squar5_261	13	1993	869	1048	3644	sym10_262	12	64283	28084	35572	122564
sym6_145	7	3888	1701	2187	7615	sym9_148	10	21504	9408	12087	41641

TABLE III: The main differences of the Trivial, MinPath, and Qmap mappers. n and g are the number of qubits and gates in an input circuit, respectively.

	Circuit optimization	ILP-based placement	Routing						Complexity
			Smart gate selection	Shortest path	MOVE operation	Multiple movement sets	Minimize latency	wrt. Classical controls	
Trivial	No	No	No	Yes	No	No	No	No	$O(g)$
MinPath	Yes	Yes	Yes	Yes	Yes	Yes	No	No	$O(g\sqrt{n}4^{\sqrt{n}})$
Qmap	Yes	Yes	Yes	Yes	Yes	Yes	Yes	Yes	$O(g\sqrt{n}4^{\sqrt{n}}) \cdot O_{schedule}$

cedure is executed for five times and the one with minimum overhead is reported.

Compared to the circuit characteristics before mapping (Table II), no matter which strategy is applied, the mapping procedure results in high overhead for most of the benchmarks as shown in Table IV. The only exceptions are the ‘benstein_v’ and ‘graycode6_47’ circuits, because some operations in these circuits can be canceled out by the optimization module in the mapper, decreasing their circuit sizes. When the trivial mapper is used, the mapping procedure leads to a high overhead in both circuit latency and total number of gates that ranges from 50% (‘graycode6_47’) to 1160% (‘xor5_254’) and from 122.9% (‘wim_266’) to 800% (‘xor5_254’), respectively.

The MinPath mapper results in an increase of the circuit latency and the total number of gates that goes from 38.9% (‘alu_v0_27’) to 260% (‘xor5_254’) and from 26.0% (‘cuccaroAdder_1b’) to 373.4% (‘rd84_142’), respectively. Finally, the proposed Qmap mapper increases the circuit latency and the total number of gates from 32.4% (‘miller_11’) to 260% (‘xor5_254’) and from 20.7% (‘cuccaroAdder_1b’) to 78.1% (‘rd32_v0’), respectively.

Furthermore, we compare the resulted overhead of these three mapping strategies as shown in Figure 6. The trivial mapper leads to the highest mapping overhead as less optimization is performed. Compared to the trivial strategy, the MinPath mapper can reduce the latency overhead and gate overhead up to 140% (‘gray6_47’) and

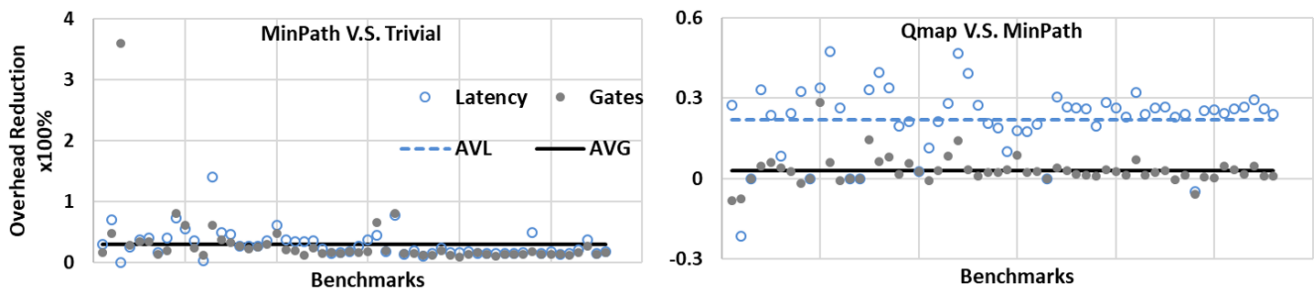


FIG. 6: Comparison of three different mapping strategies. Overhead reduction (left) when comparing the MinPath mapper to the trivial mapper and (right) when comparing Qmap to MinPath. Benchmarks are in the horizontal axis and listed in their appearing order in Table II.

360% (`'benstein_vazirani'`), respectively. The average latency (AVL) reduction and average gate (AVG) reduction are 30% and 30.2%, respectively. Moreover, the proposed Qmap mapper has lower or equal overhead than the MinPath mapper in terms of both circuit latency and number of gates for 96.4% and 87.5% of the benchmarks, respectively. More specifically, Qmap can reduce the latency overhead up to 47.3% (`'decod24_b'`) and decrease the gate overhead up to 28.6% (`'cuccaroMultiply'`) compared to the MinPath mapping strategy. The average latency (AVL) reduction and average gate (AVG) reduction are 22% and 3.0%, respectively. This is because the router in the MinPath mapper only considers the qubit connectivity limitation and minimizes the number of operations, that is, it randomly selects a movement set that has minimum number of operations to move qubits to be neighbours. The gate duration and classical constraints will only be taken into account by a later module (such as the global scheduler in this work and the OpenPulse in IBM Qiskit [16]). In comparison, the router in Qmap uses the proposed resource-constrained scheduling approach as base and evaluates more minimum-weight movement sets to select one which minimally extends the circuit latency (Section IV).

D. Scalability and runtime

As discussed in Section IV, the complexity of the proposed resource-constrained scheduling heuristic in the worst case is still polynomial, making it applicable to large-scale quantum circuits. The complexity of the routing heuristic is polynomial in terms of the number of gates but scales sub-exponentially with the number of qubits in a given circuit when using the Qmap and MinPath strategies.

We have tested three mapping strategies (Trivial, MinPath, Qmap) for different sizes of benchmarks, in which the number of qubits ranges from 3 to 16 and the two-qubit gate number from 5 to 62483. The runtime (in seconds) that different mappers requires for mapping each benchmark on the Surface-17 processor can be found in

Table IV, which is measured by the CPU time that the entire mapping procedure takes, excluding the time the ILP-based initial placement takes. As expected, the mapper that performs more optimizations and evaluates more movement sets has a longer runtime. In this case, the trivial mapper has the shortest execution time whereas the Qmap takes the longest time. For example, when mapping the largest benchmark `'sym10_262'` with 62483 gates onto the Surface-17 processor, the trivial and the Qmap mappers take 72.8 seconds and 9083.4 seconds, respectively.

Based on the complexity analysis and the experimental results, we can conclude that Qmap is scalable in terms of large number of gates. However, our experiments only use benchmarks which have less than 20 qubits. Therefore, its scalability with the number of qubits needs to be further investigated. Moreover, one may need to make a compromise between mapping performance and runtime for large-scale benchmarks.

E. SWAPs versus MOVES

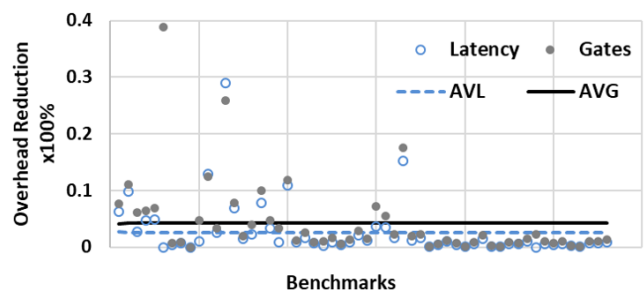


FIG. 7: Reduction of mapping overhead when using MOVES if possible compared to when only using SWAPs. Benchmarks are in the horizontal axis and listed in their appearing order in Table II. The average latency (AVL) reduction and average gate (AVG) reduction are 2.76% and 4.21%, respectively.

As mentioned in Section II, a SWAP gate is implemented by three consecutive CNOT gates whereas a MOVE operation is implemented by two consecutive CNOT gates but requiring an ancilla qubit in the state $|0\rangle$. Therefore, if there are available ancilla qubits (qubits that are not used for computation), then it is preferable to use MOVE operations rather than SWAP gates, which helps to reduce the mapping overhead. In this section, we evaluate the benefit of using MOVE operations instead of only using SWAPs. We map the benchmarks in Table II onto the Surface-17 processor using the MinPath mapper. Different from the setups in Table IV, to have a fair comparison between using MOVES if possible and only using SWAPs, in this case the native initial placement is applied and the first movement set is always selected. With the same qubit overhead, the mapping with MOVES can reduce the number of gates up to 38.9% ('bestein_vazirani') and the circuit latency up to 29% ('graycode6_47') compared to the mapping with only SWAPs as shown in Figure 7. The latency reduction and gate reduction are higher than 1% for around 48.2% and 64.3% of the benchmarks, respectively.

VI. RELATED WORK

To achieve the shortest circuit latency and provide precise timing information to generate correct control signals, schedulers that consider actual gate duration should be developed. Furthermore, the control electronic constraints that can be very restrictive especially when scaling-up quantum processors, should also be taken into account to allow valid execution of quantum applications. As discussed previously, most of prior mapping works [6, 11–23] only focus on the primitive gate set and qubit connectivity constraints. The output circuits from prior mappers need to be further scheduled with respect with the gate duration and classical control constraints, which is less optimal than the Qmap mapper as shown in Section V. Moreover, they all use SWAP operations for moving qubits when targeting superconducting quantum processors. In addition, so far no mapper has been developed for more scalable quantum processors such as the Surface-17 processor presented in [27, 43]. Although this type of processors has been designed with the aim of building a large qubit array capable of performing fault-tolerant quantum computations based on surface code, it can be also used for running quantum algorithms in a near-term implementation.

Many existing mapping algorithms [6, 11–26] and this paper use either the number of inserted movement operations or the circuit depth/latency as optimization metrics. Although all these metrics affect the success probability of a quantum circuit, an analysis on which ones are more critical to be minimized is required. Recent works [19, 21, 22, 40, 41, 44] suggest to choose the routing path based on the fidelity of the two-qubit gates along the path as they are used to implement the movements

(noise-aware mapper). However, the reliability of a path is calculated by simply multiplying the fidelity of each gate without considering error propagation and decoherence, which makes this metric incomplete and not very accurate and it thus sometimes fails in predicting the most reliable route [22]. A more accurate metric that can well represent success probability and also can be easily used by the mapping procedure needs to be developed.

VII. CONCLUSION AND DISCUSSION

In this work, we have presented a mapper called Qmap to make quantum circuits executable on the Surface-17 superconducting processor. It takes into account common processor constraints such as the primitive gate set and qubit connectivity, as well as actual gate duration and classical control electronic restrictions as it minimizes the circuit latency. Qmap has been embedded in the OpenQL compiler and consists of several modules, including qubit initial placement, resource-constrained list scheduling with polynomial complexity, qubit routing, and gate decomposition and optimization. The evaluation results show that the proposed timing and resource-aware mapper results in lower overhead in terms of both circuit latency and number of gates compared to the prior mapping strategy (MinPath) that minimizes the number of operations in the routing process and then reschedules the circuits with respect to the actual gate duration and classical control constraints. However, the complexity of the routing algorithm in Qmap scales sub-exponentially with the number of qubits in the input circuit. Future work can reduce its complexity by only evaluating the shortest paths where less qubits were, are or will be busy in the past, current, or coming cycles.

Furthermore, Qmap can be applied to different processors by only changing their corresponding hardware characteristics in the configuration file. We will investigate the performance of Qmap on other NISQ processors and compare it with prior works in the future. In addition, more mapping metrics need to be investigated and included in the mapper. Note that what parameter(s) to optimise during the mapping might depend on the characteristics of the target quantum processor. In addition, our mapping approach is based on the compilation of quantum circuits at the gate level. Although it generates valid instructions with precise timing, they still need to be further translated into appropriate signals that control the qubits by the microarchitecture proposed in [42]. A different approach is to directly compile quantum algorithms to control pulses [45]. Further work will compare both solutions and investigate the trade-off of allocating mapping tasks to the compiler and the microarchitecture.

ACKNOWLEDGMENTS

The authors would like to thank Xiang Fu and Adriaan Rol for useful discussions. The authors acknowledge sup-

port from the Intel Corporation. LLL also acknowledges funding from the China Scholarship Council.

-
- [1] J. Preskill, *Quantum* **2**, 79 (2018).
- [2] R. P. Feynman, *International Journal of Theoretical Physics* **21**, 467 (1982).
- [3] M. Kjaergaard, M. E. Schwartz, J. Braumüller, P. Krantz, J. I.-J. Wang, S. Gustavsson, and W. D. Oliver, arXiv:1905.13641 (2019).
- [4] IBM, “Quantum experience,” <https://www.research.ibm.com/ibm-q/> (2017).
- [5] S. Boixo, S. V. Isakov, V. N. Smelyanskiy, R. Babbush, N. Ding, Z. Jiang, M. J. Bremner, J. M. Martinis, and H. Neven, *Nature Physics* **14**, 595 (2018).
- [6] Rigetti, “Rigetti forest,” <https://www.rigetti.com/forest> (2018).
- [7] C. D. Hill, E. Peretz, S. J. Hile, M. G. House, M. Fuechsle, S. Rogge, M. Y. Simmons, and L. C. Hollenberg, *Science advances* **1**, e1500707 (2015).
- [8] R. Li, L. Petit, D. P. Franke, J. P. Dehollain, J. Helsen, M. Steudtner, N. K. Thomas, Z. R. Yoscovits, K. J. Singh, S. Wehner, *et al.*, *Science advances* **4**, eaar3960 (2018).
- [9] S. Asaad, C. Dickel, N. K. Langford, S. Poletto, A. Bruno, M. A. Rol, D. Deurloo, and L. DiCarlo, *npj Quantum Information* **2**, 16029 (2016).
- [10] D. C. McKay, T. Alexander, L. Bello, M. J. Biercuk, L. Bishop, J. Chen, J. M. Chow, A. D. Córcoles, D. Egger, S. Filipp, *et al.*, arXiv:1809.03452 (2018).
- [11] M. Yazdani, M. S. Zamani, and M. Sedighi, *Quantum information processing* **12**, 3239 (2013).
- [12] A. Lye, R. Wille, and R. Drechsler, in *The 20th Asia and South Pacific Design Automation Conference (ASPDAC)* (IEEE, 2015) pp. 178–183.
- [13] R. Wille, O. Keszoce, M. Walter, P. Rohrs, A. Chattopadhyay, and R. Drechsler, in *2016 21st Asia and South Pacific Design Automation Conference (ASPDAC)* (IEEE, 2016) pp. 292–297.
- [14] A. Farghadan and N. Mohammadzadeh, *International Journal of Circuit Theory and Applications* **45**, 989 (2017).
- [15] S. Herbert and A. Sengupta, arXiv:1812.11619 (2018).
- [16] H. Abraham, AduOffei, I. Y. Akhalwaya, G. Aleksandrowicz, *et al.*, “Qiskit: An open-source framework for quantum computing,” (2019).
- [17] A. Zulehner, A. Paler, and R. Wille, *IEEE Transactions on Computer-Aided Design of Integrated Circuits and Systems* (2018).
- [18] M. Y. Siraichi, V. F. d. Santos, S. Collange, and F. M. Q. Pereira, in *Proceedings of the 2018 International Symposium on Code Generation and Optimization* (ACM, 2018) pp. 113–125.
- [19] W. Finigan, M. Cubeddu, T. Lively, J. Flick, and P. Narang, arXiv:1810.08291 (2018).
- [20] G. Li, Y. Ding, and Y. Xie, in *Proceedings of the Twenty-Fourth International Conference on Architectural Support for Programming Languages and Operating Systems* (ACM, 2019) pp. 1001–1014.
- [21] S. S. Tannu and M. K. Qureshi, in *Proceedings of the Twenty-Fourth International Conference on Architectural Support for Programming Languages and Operating Systems* (ACM, 2019) pp. 987–999.
- [22] S. Nishio, Y. Pan, T. Satoh, H. Amano, and R. Van Meter, arXiv:1903.10963 (2019).
- [23] A. Cowtan, S. Dilkes, R. Duncan, A. Krajenbrink, W. Simmons, and S. Sivarajah, arXiv:1902.08091 (2019).
- [24] D. Venturelli, M. Do, E. Rieffel, and J. Frank, *Quantum Science and Technology* **3**, 025004 (2018).
- [25] K. E. Booth, M. Do, J. C. Beck, E. Rieffel, D. Venturelli, and J. Frank, in *Twenty-Eighth International Conference on Automated Planning and Scheduling* (2018).
- [26] D. Venturelli, M. Do, B. O’Gorman, J. Frank, E. Rieffel, K. E. Booth, T. Nguyen, P. Narayan, and S. Nanda, (2019).
- [27] R. Versluis, S. Poletto, N. Khammassi, B. Tarasinski, N. Haider, D. J. Michalak, A. Bruno, K. Bertels, and L. DiCarlo, *Phys. Rev. Applied* **8**, 034021 (2017).
- [28] N. Khammassi, I. Ashraf, J. v. Someren, R. Nane, A. Krol, M. A. Rol, L. Lao, K. Bertels, and C. G. Almudever, arXiv:2005.13283 (2020).
- [29] R. Wille, D. Große, L. Teuber, G. W. Dueck, and R. Drechsler, in *38th International Symposium on Multiple Valued Logic (ismvl 2008)* (IEEE, 2008) pp. 220–225.
- [30] C. C. Lin, A. Chakrabarti, and N. K. Jha, *ACM Journal on Emerging Technologies in Computing Systems* **11**, 7 (2014).
- [31] T. E. O’Brien, B. Tarasinski, and L. DiCarlo, *npj Quantum Information* **3**, 39 (2017).
- [32] J. E. Kelley Jr and M. R. Walker, in *Papers presented at the December 1-3, 1959, eastern joint IRE-AIEE-ACM computer conference* (ACM, 1959) pp. 160–173.
- [33] J. Blazewicz, J. K. Lenstra, and A. R. Kan, *Discrete applied mathematics* **5**, 11 (1983).
- [34] N. Khammassi, G. G. Guerreschi, I. Ashraf, J. W. Hogaboam, C. G. Almudever, and K. Bertels, arXiv:1805.09607 (2018).
- [35] N. Khammassi, I. Ashraf, X. Fu, C. G. Almudéver, and K. Bertels, in *Design, Automation & Test in Europe Conference & Exhibition (DATE), 2017* (IEEE, 2017) pp. 464–469.
- [36] X. Fu, L. Riesebo, M. A. rOL, J. van Straten, J. van Someren, N. Khammassi, I. Ashraf, R. Vermeulen, V. Newsum, K. Loh, *et al.*, in *2019 IEEE International Symposium on High Performance Computer Architecture (HPCA)* (IEEE, 2019) pp. 224–237.
- [37] M. J. Dousti, A. Shafaei, and M. Pedram, in *Proceedings of the 24th edition of the great lakes symposium on VLSI* (ACM, 2014) pp. 117–122.
- [38] L. Lao, B. van Wee, I. Ashraf, J. van Someren, N. Khammassi, K. Bertels, and C. G. Almudever, *Quantum Science and Technology* **4**, 015005 (2019).
- [39] M. J. Dousti and M. Pedram, in *Proceedings of the 50th*

- Annual Design Automation Conference (DAC)* (ACM, 2013) p. 42.
- [40] P. Murali, N. M. Linke, M. Martonosi, A. J. Abhari, N. H. Nguyen, and C. H. Alderete, in *Proceedings of the 46th International Symposium on Computer Architecture* (2019) pp. 527–540.
- [41] P. Murali, J. M. Baker, A. Javadi-Abhari, F. T. Chong, and M. Martonosi, in *Proceedings of the Twenty-Fourth International Conference on Architectural Support for Programming Languages and Operating Systems* (2019) pp. 1015–1029.
- [42] X. Fu, M. A. Rol, C. C. Bultink, J. van Someren, N. Khammassi, I. Ashraf, R. F. L. Vermeulen, J. C. de Sterke, W. J. Vlothuizen, R. N. Schouten, C. G. Al-mudever, L. DiCarlo, and K. Bertels, in *Proceedings of the 50th Annual IEEE/ACM International Symposium on Microarchitecture (MICRO-50)* (IEEE/ACM, 2017) pp. 813–825.
- [43] Intel, “Intel newsroom,” <https://newsroom.intel.com/press-kits/quantum-computing/#intel-qutech> (2019).
- [44] N. M. Linke, D. Maslov, M. Roetteler, S. Debnath, C. Figgatt, K. A. Landsman, K. Wright, and C. Monroe, *Proceedings of the National Academy of Sciences* **114**, 3305 (2017).
- [45] Y. Shi, N. Leung, P. Gokhale, Z. Rossi, D. I. Schuster, H. Hoffmann, and F. T. Chong, in *Proceedings of the Twenty-Fourth International Conference on Architectural Support for Programming Languages and Operating Systems* (ACM, 2019) pp. 1031–1044.

TABLE IV: The results of mapping quantum benchmarks to the Surface-17 processor, including the total number of gates and the number of two-qubit gates (CZs) in the mapped output circuits, the circuit latency in cycles (20 ns per cycle), the numbers of inserted SWAP (SWs) and MOVE (MVs) operations, and the CPU time that mapping takes in seconds.

Benchmarks	The Trivial mapper						The MinPath mapper						The Qmap mapper					
	Latency	Gates	CZs	SWs	MVs	Time	Latency	Gates	CZs	SWs	MVs	Time	Latency	Gates	CZs	SWS	MVs	Time
alu_bdd_288	335	393	113	25	0	0.06365	286	341	100	16	7	1.7313	254	362	109	15	13	1.77362
alu_v0_27	166	188	56	13	0	0.0353	100	116	30	3	2	4.20968	106	122	34	3	4	4.13529
benstein_vazirani	36	45	10	3	0	0.01667	36	9	1	0	0	0.01051	36	9	1	0	0	0.01135
4gt12_v1_89	931	1191	346	82	0	0.19592	811	917	270	54	4	25.6367	690	886	259	51	3	26.0342
4gt4_v0_72	1124	1416	413	100	0	0.2555	884	1018	296	55	9	4.40794	788	973	273	52	2	4.628
4mod5_bdd_287	298	339	100	23	0	0.07120	234	247	71	10	5	18.7469	226	240	69	10	4	19.5225
cm42a_207	7167	8782	2532	587	0	1.42467	6499	7887	2352	517	15	611.534	5713	7724	2301	494	24	535.889
cnt3_5_180	1985	2491	725	170	0	0.38054	1480	2103	623	136	0	25.0301	1236	2132	641	142	0	25.6028
cuccaroAdder_1b	175	171	50	11	0	0.03036	90	92	23	0	3	0.2521	90	92	23	0	3	0.28906
cuccaroMultiply	417	427	122	30	0	0.06122	260	274	74	10	6	2.05933	217	246	64	6	7	2.09601
decod24_bdd	315	375	110	26	0	0.06353	253	301	90	14	8	1.38109	201	287	83	15	3	1.46449
decod24_enable	1342	1607	467	106	0	0.23441	1324	1464	434	95	0	28.704	1151	1474	434	95	0	28.7617
graycode6_47	30	31	11	2	0	0.00898	16	15	5	0	0	5.83973	16	15	5	0	0	5.8601
ham3_102	79	87	26	5	0	0.01126	60	62	17	2	0	0.15724	60	62	17	2	0	0.22297
millier_11	199	222	65	14	0	0.02856	156	166	46	3	7	0.19096	139	149	39	0	8	0.27471
mini_alu_167	1144	1431	414	96	0	0.21319	985	1120	309	61	0	29.411	818	1068	294	56	0	28.5271
mod5adder_127	2229	2744	794	185	0	0.44677	1908	2240	645	130	8	7.0105	1618	2104	598	109	16	7.4544
mod8_10_177	1819	2285	661	155	0	0.36898	1570	1808	530	102	14	2.26425	1434	1786	518	106	2	2.53567
one_two_three	287	346	101	23	0	0.05446	235	263	76	12	4	6.18516	215	252	70	10	4	6.41456
rd32_v0_66	168	184	55	13	0	0.02766	105	113	32	4	2	1.65692	104	111	31	1	6	1.71454
rd53_311	1183	1514	448	108	0	0.24811	909	1249	370	78	6	0.32513	856	1257	375	81	4	0.67113
rd73_140	970	1198	350	82	0	0.19047	751	1010	300	62	5	20.682	662	988	292	52	16	20.3441
rd84_142	1385	1804	526	124	0	0.30129	1044	1624	481	109	0	20.7494	861	1516	448	98	0	21.1735
sf_274	3351	3892	1137	267	0	0.67493	2705	3157	926	178	28	40.0639	2151	2822	818	104	85	41.2879
shor_15	15082	19608	5472	1228	0	4.33023	13460	17464	5046	1028	87	2.45284	11217	17058	4924	982	95	14.6928
sqrt8_260	12708	16131	4719	1135	0	3.49803	11626	14041	4231	953	29	4.12037	10020	13944	4216	956	17	13.2009
squar5_261	7865	10178	2951	694	0	2.17597	7198	8922	2663	594	6	3.48788	6468	8764	2630	585	3	7.76352
sym6_145	15466	19266	5583	1294	0	4.12125	14094	16427	4872	965	138	3.94839	12873	16145	4787	970	88	16.7757
sym9_146	1250	1721	499	117	0	0.30173	1040	1493	447	93	10	21.1801	980	1456	431	91	5	21.6935
sys6_v0_111	859	1142	338	80	0	0.24816	640	976	290	62	3	21.1563	573	909	267	49	11	21.1608
vbeAdder_2b	332	468	135	31	0	0.09799	236	300	79	9	5	0.16455	215	298	80	6	10	0.1938
wim_266	3941	5084	1474	349	0	0.98658	3546	4289	1273	272	15	13.0377	3190	4203	1254	265	16	13.5583
xor5_254	63	63	23	6	0	0.01135	18	18	8	1	0	29.7578	18	18	8	1	0	29.2384
z4_268	12341	15792	4598	1085	0	3.19178	11463	13962	4178	905	60	818.036	9704	13537	4088	887	42	869.445
adr4_197	14296	18110	5287	1263	0	3.38715	12772	15868	4780	1082	18	1.67818	11070	15496	4685	1021	62	10.924
9symml_195	142144	182319	53224	12664	0	36.5722	134023	164219	49485	11167	376	16.642	116118	162001	49154	11282	38	2332.7
clip_206	139948	180243	52809	12679	0	40.1273	128597	162421	49227	11379	159	17.44	111253	160880	49090	11268	257	2587.99
cm152a_212	5166	6320	1834	434	0	1.3859	4508	5347	1586	346	8	0.66896	4086	5306	1591	353	0	3.53968
cm85a_209	48394	61007	17886	4300	0	14.2237	44110	54845	16654	3832	86	6.49007	37839	53363	16224	3716	45	389.036
col4_215	75821	99108	29218	7126	0	20.9755	68064	92308	28381	6837	15	10.8777	57968	90267	27787	6615	51	1044.04
cycle10_2_110	25607	31630	9236	2196	0	7.12406	23070	28148	8460	1904	50	3.26144	20458	27897	8471	1899	63	106.071
dc1_220	7740	9845	2867	678	0	2.62955	7116	8575	2574	567	20	1.45486	5979	8117	2444	481	84	8.51783
dc2_222	39466	50396	14754	3541	0	12.5991	36113	44864	13547	3100	58	5.16826	31796	44379	13520	3077	79	268.637
dist_223	156674	201426	58891	14089	0	40.4085	144079	183197	55613	12757	359	55.0312	124031	179639	54717	12599	148	3550.7
ham15_107	36221	45826	13356	3166	0	10.1604	33368	40721	12257	2797	4	5.74947	28906	39762	12030	2704	30	193.48
life_238	92286	117371	34238	8146	0	30.3595	85068	104447	31370	7134	84	14.0716	75462	104689	31920	7324	74	1364.49
max46_240	111978	141438	41211	9789	0	35.6086	101798	125209	37631	8375	331	16.8426	89164	123895	37565	8217	535	1840.89
mini_alu_305	767	862	254	59	0	0.16079	505	741	228	35	23	0.19804	518	775	242	41	21	0.40925
misex1_241	19670	24793	7206	1702	0	5.75472	18143	22002	6577	1479	20	3.13745	15892	21883	6588	1480	24	53.4152
pm1_249	7167	8782	2532	587	0	2.3615	6446	7793	2314	499	23	1.48028	5629	7774	2331	504	24	6.86838
radd_250	13254	16700	4867	1154	0	4.11447	12291	14955	4516	979	87	2.43807	10798	14408	4363	948	57	24.0061
root_255	71310	91873	26882	6463	0	20.7858	64948	82599	24991	5824	13	11.4199	55963	80542	24520	5627	73	844.114
sqn_258	43328	53252	15529	3690	0	11.7106	38165	46370	13908	3019	196	6.55198	33010	45801	13815	2984	202	270.981
square_root_7	35769	44042	12896	3269	0	10.6409	27419	34333	10274	2371	36	50077.7	23203	33088	9845	2184	102	46862.9
sym10_262	269200	340622	99658	23858	0	72.7567	247750	305153	92270	21030	548	42.2372	215185	303141	92326	20986	642	9083.41
sym9_148	87919	110393	32127	7573	0	27.4377	79881	95215	28378	6152	257	14.4444	70756	94656	28462	6182	254	800.226